JOURNAL OF Materials CHEMISTRY

On the new oxovanadium phosphate $NaZnVOPO_4(HPO_4)$ obtained at 510 K from hydrothermal treatment

E. Le Fur, Y. Moreno† and J. Y. Pivan*

Laboratoire de Physicochimie, Ecole Nationale Supérieure de Chimie de Rennes, Campus de Beaulieu, Avenue du Général Leclerc, 35700 Rennes, France. E-mail: jean-yves.pivan@ensc-rennes.fr

Received 13th December 2000, Accepted 8th March 2001
First published as an Advance Article on the web 20th April 2001

Pale blue powders of $NaZnVOPO_4(HPO_4)$ were prepared in quantitative yield from hydrothermal treatments. The structure of $NaZnVOPO_4(HPO_4)$ was solved from single crystal X-ray diffraction data in the centrosymmetric monoclinic space group $P2_1/c$ (no. 14), $a=8.5441(2)$ Å, $b=8.9831(2)$ Å, $c=9.0836(2)$ Å, $\beta=91.241(1)^\circ$, $Z=4$ ($R_1(F_o)=0.026$, $wR_2(F_o^2)=0.068$). The structure results from the hetero-condensation of distorted octahedra VO_6 with tetrahedra H_xPO_4 and ZnO_4 by sharing apices and edges. The remaining voids of the 3D framework $[ZnVOPO_4(HPO_4)]^-$ located in tunnels that run along [011] are occupied by sodium ions. The title compound dehydrates at $T\sim770$ K with an overall weight loss of $\sim2.3\%$ consistent with the structural results. The crystal chemical relationships with $Na_3VOPO_4(HPO_4)$ and the high-temperature phase $SrZnVO(PO_4)_2$ are discussed.

Introduction

Intensive work has been devoted to the preparation of new oxovanadium phosphates (referred to herein as MVPOs) since vanadyl pyrophosphate $(VO)_2P_2O_7$ has been discovered to be an efficient catalyst for the oxidation of light hydrocarbons to maleic anhydride.[1] As a result, a great number of new MVPOs has been prepared over the last ten years by using different synthetic routes. The most promising one is indisputably the hydrothermal route insofar as (i) open frameworks are more easily attainable, (ii) the phosphate groups can be present as PO_4^{3-}, HPO_4^{2-} and(or) $H_2PO_4^-$ that allow one to obtain original solids after thermal treatments, (iii) unstable counter-ions M^{x+} such as organic cations and water molecules can be encapsulated in the frameworks that are easily removed upon heating to recover the free pore volume. The "black box nature inherent in the hydrothermal reactor" makes *in situ* analyses difficult to perform and most of the research teams agree nowadays that the mechanisms involved during hydrothermal syntheses remain obscure.[2] Nevertheless, new analytical techniques are currently emerging[3] of which the synchrotron radiation sources open up promising perspectives to get analytical data that were unthinkable previously..[4] Despite the impossibility to explain with certainty the synthetic pathways, chemists have adopted various but similar strategies to attain reproducibility with quantitative yields. Of the different parameters that control the syntheses, our recent results have clearly demonstrated that kinetic effects are very important in that different MVPOs solids were isolated from identical starting mixtures depending upon the reaction time. So, investigations were undertaken by lengthening the reaction time, resulting in new MVPO phases. In this context, the present paper deals with the synthesis, crystal structure and thermal behaviour of the three-dimensional $NaZnVO-PO_4(HPO_4)$

†On leave from Facultad de Ciencias Quimicas y Farmaceuticas, Universidad de Chile, Santiago, Chile.

Experimental section

Synthesis

Mixtures of M_2CO_3 (0.150 g), V_2O_5 (0.154 g), Zn^0 (0.115 g) were added to 5 ml of a solution ~1.5 M H_3PO_4, sealed in a 23 ml Teflon lined acid digestion bomb (Parr Instruments), then heated at 240 °C under autogenous pressure for 8 days. After slowly cooling to room temperature, the reaction products were filtered off, rinsed with distilled water and dried in air in a furnace maintained at 100 °C for 24 h. Prior to subsequent analyses, the reaction products were checked by visual examination under the microscope and appeared as pale blue platelet single crystals without visible by-products.

X-Ray diffraction

The crystals were crushed to powder and analysed by X-ray diffraction using λ(Cu Kα) = 1.54178 Å. All the diffraction peaks of the resulting X-ray pattern were indexed with DICVOL91[5] on the basis of a monoclinic unit cell with the parameters $a=9.083(3)$ Å, $b=9.008(3)$ Å, $c=8.543(1)$ Å, $\beta=91.19(3)^\circ$. Single crystal studies were made at room temperature using an Enraf-Nonius diffractometer with graphite monochromated Mo Kα radiation ($\lambda=0.71073$ Å) equipped with a CCD detector that confirmed the results obtained from the X-ray powder diffraction analyses. During the experiment the goniometer and detector angular settings were optimised with the help of the program COLLECT and the intensity data collection was conducted in the ω–ϕ scanning mode.[6] The crystal to detector distance was 25 mm. The unit cell and the orientation matrix were refined using the entire data set of 11079 reflections recorded up to $2\theta=74^\circ$. The diffraction spots were measured in full with a high accuracy as indicated by the statistical indicators ($\chi^2<1$) obtained from the program COLLECT.[6] A set of 214 frames was collected for a total exposure of 174 min. Lorentz-polarization correction and peak integration were performed with DENZO and the data set was scaled using SCALEPACK.[6] The main crystallographic data and conditions for structure analysis are listed in Table 1 together with the reliability factors at the end of refinement. The systematic absences ($h0l$, $l=2n+1$; $0k0$, $k=2n+1$) indicate

Table 1 Crystal data for $NaZnVOPO_4(HPO_4)$

Empirical formula	$NaZnVP_2O_9H$
Crystal system	monoclinic
Crystal size/mm^3	$0.13 \times 0.11 \times 0.05$
Space group	$P2_1/c$ (no. 14)
Recording temperature/K	300
Unit cell dimensions	$a = 8.5441(2)$ Å
	$b = 8.9831(2)$ Å
	$c = 9.0836(2)$ Å
	$\beta = 91.241(1)^\circ$
Volume/Å^3	697.03(3)
Z	4
Formula weight/g mol^{-1}	1384.99
Density (calc.)/g cm^{-3}	3.30
Absorption coefficient/cm^{-1}	53.3
Residuals[a]	$R_1 = 0.0259$, $wR_2 = 0.0680$
GooF	1.228
Min., max. /e Å^{-3}	-0.613, $+0.655$

[a] $R_1 = \Sigma\|\|F_o\|-\|F_c\|\|/\Sigma\|F_o\|$; $wR_2 = [\Sigma w(\|F_o\|^2-\|F_c\|^2)/\Sigma w\|F_o\|^2]^{1/2}$ with $w = 1/[\sigma^2(F_o^2 + 2.6144P^2]$; $P = (\max(F_o^2, 0) + 2F_c^2)/3$.

Table 2 Atomic positional coordinates and equivalent displacement parameters U_{eq}(Å$^2 \times 10^4$) for $NaZnVOPO_4(HPO_4)$

Atom	x	y	z	U_{eq}
Zn	0.15008(4)	0.33834(4)	0.58506(4)	1.04(1)
V	0.56188(6)	0.00057(5)	0.74441(5)	0.64(1)
P1	0.48937(8)	0.25154(8)	0.00164(7)	0.59(1)
P2	0.96269(9)	0.12864(8)	0.77624(8)	0.90(2)
Na	0.8072(2)	0.0302(1)	0.4782(1)	1.65(3)
O1	0.0842(3)	0.1033(3)	0.8937(2)	1.90(5)
O2	0.8456(2)	0.9992(2)	0.7625(2)	1.01(4)
O3	0.5849(2)	0.1511(2)	0.9034(2)	1.03(4)
O4	0.6067(2)	0.1607(2)	0.5986(2)	0.93(4)
O5	0.6217(2)	0.8546(2)	0.5848(2)	0.96(4)
O6	0.3767(3)	0.9838(3)	0.7299(2)	1.54(4)
O7	0.0356(3)	0.1542(2)	0.6260(2)	1.29(4)
O8	0.6184(2)	0.8410(2)	0.8965(2)	0.90(4)
O9	0.8669(3)	0.2745(3)	0.8132(3)	2.14(5)

the centrosymmetric space group $P2_1/c$ (no. 14). The starting structure model was extracted by direct methods using SIR97[7] and the refinements were made on F_o^2 with SHELXL-97.[8] The entire structure model (non-hydrogen atoms) was readily obtained from successive difference Fourier maps. At the end of refinement, anisotropic displacement parameters for non-hydrogen atoms and the extinction coefficient were allowed to vary, resulting in the final reliability factors $R_1(F_o) \sim 0.026$, $wR_2(F_o^2) \sim 0.068$ for 2033 unique reflections (1883 $I \geqslant 2\sigma(I)$ and 128 variable parameters). In order to balance charge, additional protons were required that were not located experimentally and were input in the final formula after accurate scrutiny of the framework counting the non-shared oxygen atoms on the phosphate groups. Atomic positional coordinates and atomic displacement parameters are given in Table 2. Selected bond distances and angles are summarised in Table 3.

CCDC reference number 155040. See http://www.rsc.org/suppdata/jm/b0/b009952j/ for crystallographic data in CIF or other electronic format

Thermogravimetric measurements

Thermal analyses, using a SHIMADZU thermogravimetric analyser, were performed on crushed samples in flowing N_2 with a heating rate of 5 °C min^{-1}. The loss of weight (2.3%) occurs in one step at 770 K and compares well with the expected value (2.7%) considering water elimination through the condensation mechanism $2HPO_4 \rightarrow P_2O_7 + H_2O$. After the heat treatments, the resulting product was recovered as a black powder, the X-ray diffraction pattern of which remains unknown.

NMR measurements

The NMR experiments were run on a ASX 300 Bruker instrument for ^{31}P and ^1H nuclei according to the acquisition conditions listed in Table 4. A high speed probe head spinning at up to 15 kHz with 4 mm rotors was used. At 15 kHz, two ^{31}P

Table 3 Main interatomic bond distances (Å) and angles (°) for $NaZnVOPO_4(HPO_4)$ with the corresponding bond valence sums Σs

Zn						
O1	1.889(2)					
O7	1.962(2)	105.6(1)				
O8	1.981(2)	110.6(1)	119.66(9)			
O2	2.001(2)	115.9(1)	118.65(9)	85.95(8)		
$\Sigma s = 2.02$						
V						
O6	1.592(2)					
O3	1.985(2)	101.9(1)				
O4	1.998(2)	102.6(1)	88.51(9)			
O5	2.028(2)	98.3(1)	159.69(9)	86.38(8)		
O8	2.042(2)	102.1(1)	88.17(8)	155.25(9)	88.29(8)	
O2	2.426(2)	174.2(1)	82.59(8)	80.97(8)	77.20(8)	74.28(8)
$\Sigma s = 4.01$						
P1						
O3	1.519(2)					
O5	1.530(2)	113.1(1)				
O4	1.538(2)	106.8(1)	111.9(1)			
O8	1.560(2)	111.3(1)	105.0(1)	108.6(1)		
$\Sigma s = 5.01$						
P2						
O1	1.490(2)					
O7	1.530(2)	111.8(1)				
O2	1.538(2)	112.6(1)	108.5(1)			
O9	1.585(2)	109.2(1)	106.7(1)	107.7(1)		
$\Sigma s = 4.97$						
Na						
O7	2.345(3)	O4	2.364(2)	O9	2.370(3)	O6	2.435(3)
O5	2.450(2)	O7	2.596(3)	O2	2.611(2)		
$\Sigma s = 1.25$						

Table 4 MAS NMR one pulse conditions for $NaZnVOPO_4(HPO_4)$ ($H_0 = 7$ T)

	^{31}P	^{1}H
Pulse length/μs	1.5	3
Dead time/μs	5	5
Resonance frequency/MHz	121.5	300
Spectral width/kHz	200	500
Reference (0 ppm)	H_3PO_4 85%	TMS
MAS spinning speed/MHz	15	15
Number of scans	1024	1024
Number of digitized points	8192	8192

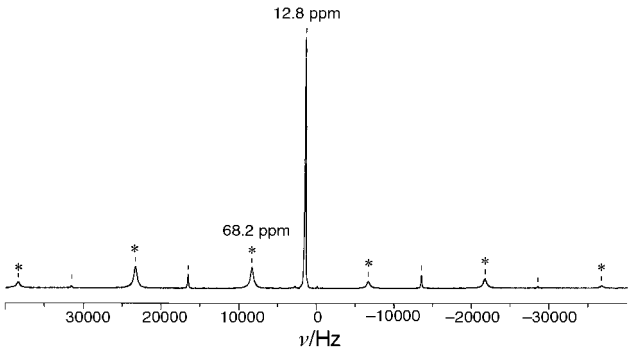

Fig. 1 Magic angle spinning ^{31}P NMR spectrum of $NaZnVOPO_4(HPO_4)$ showing two shifted signals.

signals were observed at $\delta^{(1)} = 12.8$ and $\delta^{(2)} = 68.2$ ppm with spinning sidebands indicative of similar dipolar couplings (Fig. 1). The two signals were decomposed as a sum of Lorentzian–Gaussian lines xG/(1−x)L with $x = 0.4$ and 0.1 respectively. The best fits were obtained for $\Delta\nu_{1/2}{}^{(1)} = 155$ Hz (∼1.3 ppm), $\Delta\delta^{(1)} = +100$ ppm and $\eta^{(1)} = 1$ (signal at 12.8 ppm); $\Delta\nu_{1/2}{}^{(2)} = 500$ Hz (∼4.2 ppm), $\Delta\delta^{(2)} = -357$ ppm and $\eta^{(2)} = 0$ (signal at 68.2 ppm) where $\Delta\nu_{1/2}$, $\Delta\delta$ represent the halfwidth of the isotropic line and chemical shift anisotropy and $\eta = (\delta_{xx} - \delta_{yy})/\delta_{zz}$ relates to the anisotropy of the chemical shift tensor. The values of η are indicative of the local symmetry at the ^{31}P nuclei. Hence the less symmetric $HPO_4{}^{2-}$ which would see one V^{IV} center was assigned to $\delta^{(1)} = 12.8$ ppm ($\eta^{(1)} = 1$) while the $PO_4{}^{3-}$ within a square planar lattice of V^{IV} centers would resonate at $\delta^{(2)} = 68.2$ ppm ($\eta^{(2)} = 0$). Assignments of the shifts agree well with previous studies made on related magnetic phosphates where magnetic exchange couplings involving phosphorus atoms occur.[9,10] Spin lattice relaxation times $T1^{(1)} = 42$ ms and $T1^{(2)} = 3.5$ ms probably depend on the chemical shift anisotropy through the equation $1/T1 \sim \alpha(\Delta\delta)^2$ as the ratio $T1^{(1)}/T1^{(2)} = 12$ compares fairly well with $[\Delta\delta^{(2)}/\Delta\delta^{(1)}]^2 \sim 13$. The integrated areas were calculated using the Bruker software Winfit[11] and were in the ratio $HPO_4{}^{2-}/PO_4{}^{3-} \sim 1$ in good agreement with the results from the structure analysis. One well resolved line is observed in the ^{1}H MAS spectrum at $\delta = +8.3$ ppm. with $\Delta\nu_{1/2} = 720$ Hz (∼2.4 ppm), $\Delta\delta = +98$ ppm, $\eta = 0.5$ and $T1 = 2.75$ ms. The signal exhibits spinning sidebands indicating strong dipolar couplings and therefore the proton is fixed at the OH group on the $HPO_4{}^{2-}$.

Structure results

The structure of $NaZnVOPO_4(HPO_4)$ is shown in Fig. 2 in projection along the [010] direction. The overall framework consists of VO_6 octahedra connected with ZnO_4 and H_xPO_4 tetrahedra. The near-neighbourhood of the vanadium ions consists of a short V=O bond length of 1.592(2) Å that is typical of the vanadyl species, a long V···O bond *trans* to the

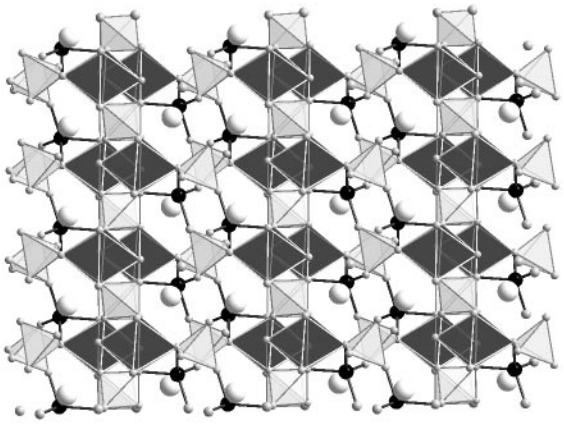

Fig. 2 View of $NaZnVOPO_4(HPO_4)$ along the [010] direction. Black polyhedra are VO_6 octahedra, open ones are PO_4 tetrahedra. White circles: Na^+, black circles: Zn^{2+}.

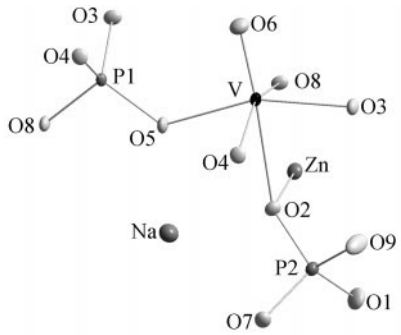

Fig. 3 View of the asymmetric unit of $NaZnVOPO_4(HPO_4)$ (ORTEP-style) showing the connectivity. Thermal ellipsoïds are at the 70% probability level.

V=O one at $d = 2.426(2)$ Å and four equatorial bonds with $\bar{d}_{V-O} = 2.013$ Å. As usually found in oxovanadium chemistry when no homo-condensation occurs, the oxygen atom of the vanadyl group (namely O6) is not shared with other polyhedra. Each VO_6 octahedron is corner-connected through the equatorial oxygen atoms (namely O3, O4, O5 and O8) (Fig. 3) to four $PO_4{}^{3-}$ groups (around P1) to form layers with composition $[VOPO_4]$ as found in the structures of the layered compounds $M_x(VOPO_4)_2{\cdot}yH_2O$.[12–21] The V–O–P bond angles within the layer $[VOPO_4]$ are in the range 128.09°–141.80°. The V=O bonds alternate up and down with respect to the layer. Additional corner-sharing VO_6/PO_4 occurs *trans* to the short V=O bond with $HPO_4{}^{2-}$ tetrahedra with the corresponding V–O–P bond angle of 130.48°. The resulting 2D framework $[VOPO_4(HPO_4)]^{3-}$ resembles very closely that reported for $Na_3VOPO_4(HPO_4)$.[22] The P–O bond lengths in the phosphate groups are in the range 1.490(2)–1.585(2) Å ($\bar{d}_{P-O} = 1.537$ Å) with an average intra-tetrahedral angle ($\bar{\alpha} = 109.4°$) very close to the ideal value. The longer P2–O9 bond distance at $d = 1.585(2)$ Å reflects the influence of a terminal OH group while the P1–O8 distance at $d = 1.560(2)$ Å takes its origin in the fact that O8 is involved in a μ_3-oxo bridge. In the title compound, the layers $[VOPO_4(HPO_4)]^{3-}$ are piled up in the same manner as are the neutral layers $[V(H_2O)OPO_4]$ in the oxovanadium phosphate hydrate $VOPO_4{\cdot}2H_2O$. This particular piling, coupled to the occurrence of $HPO_4{}^{2-}$ groups, generates tetrahedral voids that are filled up by the Zn^{2+} ions with $\bar{d}_{Zn-O} = 1.958$ Å and $\bar{\alpha}_{O-Zn-O} = 109.4°$. Each ZnO_4 tetrahedron connects *via* corner- and edge-sharing to adjacent polyhedra through two μ_3-and two μ_2-oxo bridges. Though $\bar{\alpha}_{O-Zn-O}$ is close to the ideal value for tetrahedral coordination, the ZnO_4 tetrahedron is strongly distorted (see Table 3) in

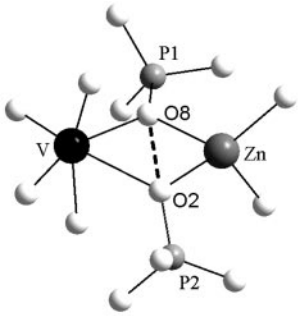

Fig. 4 The ZnO_4/VO_6 edge-sharing showing the μ_3-oxo bridges at O2 and O8.

relation with the ZnO_4/VO_6 edge-sharing (Fig. 4). It is worthwhile to note that the oxygen atoms at the μ_3-oxo bridges (namely O2 and O8) are making the longer bond lengths for the different polyhedra. The resulting negatively charged 3D framework $[ZnVOPO_4(HPO_4)]^-$ exhibits tunnels with a pentagonal cross-section and approximate aperture $\phi \sim 3$ Å that run roughly along the [011] direction. The OH groups of the HPO_4^{2-} are directed towards the centre of the tunnels. The sodium ions are located inside the tunnels and are surrounded by seven oxygen atoms at distances in the range 2.345(3) Å–2.611(2) Å. Bond valence sum calculations[23] give formal oxidation states in good agreement with the expected values for V^{4+} ($\Sigma s = 4.01$), P^{5+} ($\Sigma s = 4.97$, 5.00), Zn^{2+} ($\Sigma s = 2.02$) and Na^+ ($\Sigma s = 1.25$).

Discussion

The structure of $NaZnVOPO_4(HPO_4)$ resembles those of $Na_3VOPO_4(HPO_4)$[22] and $SrZnVO(PO_4)_2$[24] as shown in Fig. 5. The main crystallographic features of the three structures are reported in Table 5. The same 2D topological units with composition $[VOPO_4(H_xPO_4)]^{(4-x)-}$ ($x = 0$, 1) occur that can be thought of as layers of $[VOPO_4]$ with additional phosphate groups oriented alternately up and down with respect to the plane of the layers. For sake of simplification, the polyhedra POLs will be referred hereafter as ^{IL}POLs (IntraLayer) if belonging to the layer $[VOPO_4]$ or ^{EL}POLs (ExtraLayer) if not. There are only $^{IL}[PO_4]/^{IL}[VO_6]$ μ_2-oxo links in the layers. The equatorial planes of the $^{IL}[VO_6]$ are parallel to the plane of the layers for $Na_3VOPO_4(HPO_4)$ and $NaZnVOPO_4(HPO_4)$ while they are rotated by about $\alpha \sim \pm 18.4°$ for $SrZnVO(PO_4)_2$. As a consequence, the layers $[VOPO_4]$ are regular for $Na_3VOPO_4(HPO_4)$ and $NaZnVOPO_4(HPO_4)$ and they are slightly corrugated for $SrZnVO(PO_4)_2$. Additionally, the ^{IL}POLs are connected to the ^{EL}POLs through μ_2-oxo bridges $^{EL}[HPO_4]/^{IL}[VO_6]$ for $Na_3VOPO_4(HPO_4)$ and $^{EL}[PO_4]/^{IL}[VO_6]$ for $SrZnVO(PO_4)_2$ or through μ_3-oxo bridges $^{EL}[HPO_4]/^{EL}[ZnO_4]/^{IL}[VO_6]$ for $NaZnVOPO_4(HPO_4)$. Whatever the nature of the links, the shared

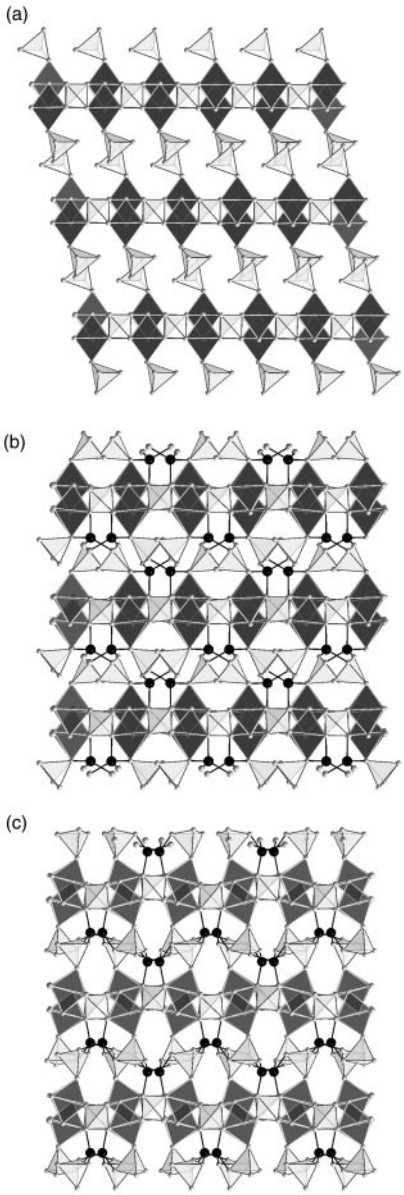

Fig. 5 Comparison of the structures of (a) $Na_3VOPO_4(HPO_4)$ viewed along [011], (b) $NaZnVOPO_4(HPO_4)$ viewed along [001] and (c) $SrZnVO(PO_4)_2$ viewed along [010]. Na^+ and Sr^{2+} are omitted for sake of clarity.

Table 5 Main crystal data for $Na_3VOPO_4(HPO_4)$, $NaZnVOPO_4(HPO_4)$ and $SrZnVO(PO_4)_2$. Units are Å (bond lengths) and ° (angles)

	$Na_3VOPO_4(HPO_4)$ min. < av. < max.	$NaZnVOPO_4(HPO_4)$ min. < av. < max.	$SrZnVO(PO_4)_2$ min. < av. < max.
$(V–V)^{short}$	4.576 < 4.632 < 4.688	4.542 < 4.639 < 4.616	4.696 < 4.708 < 4.721
$(V–V)^{long}$	6.264 < 6.336 < 6.407	6.395 < 6.388 < 6.380	6.357 < 6.391 < 6.426
V=O	1.626	1.592	1.599
V···O	2.295	2.426	2.189
$(V–O)_{eq}$	1.928 < 1.991 < 2.02	1.985 < 2.013 < 2.042	1.971 < 2.023 < 2.110
$(V_i–O–P_i)$	130.7 < 131.9 < 133.5	126.5 < 131.6 < 141.8	124.1 < 134.3 < 148.8
$(V_i–O–P_e)$	131.2	130.5	153.3
$(P–O)_i$	1.511 < 1.531 < 1.539	1.519 < 1.537 < 1.560	1.529 < 1.544 < 1.583
$(P–O)_e$	1.516 < 1.551 < 1.583	1.490 < 1.536 < 1.585	1.526 < 1.537 < 1.552
$(O–P–O)_i$	104.8 < 108.2 < 112.6	105.0 < 109.4 < 113.1	102.8 < 109.5 < 115.6
$(O–P–O)_e$	106.8 < 109.4 < 113.3	106.7 < 109.4 < 112.6	106.5 < 109.4 < 112.0
(Zn–O)		1.889 < 1.958 < 2.001	1.932 < 1.952 < 1.974
(O–Zn–O)		85.9 < 109.4 < 119.7	94.8 < 109.4 < 123.4

The (V–V) distances are the distances within the $VOPO_4$ layers, the subscripts i and e represent intralayer and extralayer respectively.

oxygen atom makes the longer V···O bonds with the corresponding bond angles $\alpha_{V-O-P}=131.19°$ for $Na_3VOPO_4(HPO_4)$, $\alpha_{V-O-P}=153.34°$ for $SrZnVO(PO_4)_2$ and $\alpha_{V-O-P}=130.48°$ for $NaZnVOPO_4(HPO_4)$. The $^{EL}[ZnO_4]$ are making three μ_2-oxo bridges $^{EL}[PO_4]/^{EL}[ZnO_4]$ and one μ_3-oxo bridge $^{IL}[PO_4]/^{EL}[ZnO_4]/^{IL}[VO_6]$ in $SrZnVO(PO_4)_2$ while they are connected *via* two μ_2-oxo bridges $^{EL}[HPO_4]/^{EL}[ZnO_4]$ and two μ_3-oxo bridges $^{IL}[PO_4]/^{EL}[ZnO_4]/^{IL}[VO_6]$ and $^{EL}[HPO_4]/^{EL}[ZnO_4]/^{IL}[VO_6]$ in $NaZnVOPO_4(HPO_4)$. As a consequence, the $^{EL}[ZnO_4]$ and $^{IL}[VO_6]$ are edge-connected in $NaZnVOPO_4(HPO_4)$ that allow one apex of the $^{EL}[HPO_4]$ to be non-shared and corresponds to the longer P–O distance ($d_{P-O}=1.585$ Å) characteristic of a P–OH terminal group. It is worth noting that all the interatomic bond distances and angles involving the oxygen atoms at the μ_3-oxo bridges are significantly modified (see Table 5). From the preceding, the connectivity is $[VOO_{5/2}][PO_{4/2}][PO_{1/2}O_3]$ for $Na_3VOPO_4(HPO_4)$, $[VOO_{4/2}O_{1/3}][PO_{4/2}][PO_{3/2}O_{1/3}][ZnO_{3/2}O_{1/3}]$ for $SrZnVO(PO_4)_2$ and $[VOO_{3/2}O_{2/3}][PO_{3/2}O_{1/3}][PO_{2/2}O_{1/3}O][ZnO_{2/2}O_{2/3}]$ for $NaZnVOPO_4(HPO_4)$. Finally, the layers are piled without net displacement in $SrZnVO(PO_4)_2$ and $NaZnVOPO_4(HPO_4)$ while they are moved from each other by $\boldsymbol{T}\sim(\boldsymbol{a}+\boldsymbol{b})/2$ in $Na_3VOPO_4(HPO_4)$. Such relative displacements of the layers has been described in detail in the majority of the cases reported for the layered compounds $M(VOPO_4)_2\cdot 4H_2O$. The topological differences between the three structures result from the different connectivity and piling: $Na_3VOPO_4(HPO_4)$ is actually layered with the negatively charged $[VOPO_4(HPO_4)]^{3-}$ held together through ionic interactions by the counterbalancing cations Na^+ while the ZnO_4 polyhedra in $SrZnVO(PO_4)_2$ and $NaZnVOPO_4(HPO_4)$ make the resulting framework three dimensional by ensuring additional connectivity between adjacent layers.

Conclusion

The new oxovanadium phosphate $NaZnVOPO_4(HPO_4)$ has been hydrothermally isolated. Its structure is three-dimensional and it has been solved from X-ray crystal intensity diffraction data recorded using a CCD detector. It cristallizes in the centrosymmetric space group $P2_1/c$ and shows structural similarities with $Na_3VOPO_4(HPO_4)$ and $SrZnVO(PO_4)_2$. The overall topology results from the heterocondensation of $[VO_6]$ distorted octahedra and $[ZnO_4]$ tetrahedra with orthophosphate units. The sodium atoms are trapped inside tunnels along [011]. The loss of weight from thermogravimetric studies have been attributed to water elimination according to condensation: $2HPO_4 \rightarrow P_2O_7+H_2O$. NMR experiments clearly distinguish PO_4^{3-} and HPO_4^{2-} and show that there is no protonic delocalization.

Acknowledgements

The authors are indebted to Dr T. Roisnel for the single crystal intensity data collection on the Kappa CCD diffractometer (Université de Rennes I, LCSIM, UMR 6511) and Dr J. Gallier for the NMR measurements. Y. Moreno benefited from a post-doctoral stage within the ECOS-Sud collaboration program (C97E01) between Chile and France.

References

1 G. Centi, F. Trifiro, J. R. Ebrer and V. M. Franchetti, *Chem. Rev.*, 1988, **88**, 55.
2 P. Amorós, M. Dolores Marcos, A. Beltrán-Porter and D. Beltrán-Porter, *Curr. Opin. Solid State Mater. Sci.*, 1999, **4**, 123 and references therein.
3 R. J. Francis and D. O'Hare, *J. Chem. Soc., Dalton Trans.*, 1998, 3133.
4 W. Clegg, *J. Chem. Soc., Dalton Trans.*, 2000, 3223.
5 D. Louër and M. Boultif, *J. Appl. Crystallogr.*, 1991, **24**, 987.
6 COLLECT, DENZO, SCALEPACK, SORTAV, Kappa CCD Program Package, Nonius BV, Delft, The Netherlands, 1998.
7 A. Altomare, M. C. Burla, M. Camalli, G. L. Cascarano, C. Giacovazzo, A. Guagliardi, A. G. G. Moliterni, G. Polidori and R. Spagna, *J. Appl. Crystallogr.*, 1999, **32**, 115.
8 G. M. Sheldrick, SHELXL-97, Program for crystal structure refinement, University of Göttingen, Germany, 1997.
9 D. Beltran-Porter, A. Beltran-Porter, P. Amorós, R. Ibañez, A. Le Bail, G. Ferey and G. Villeneuve, *Eur. J. Solid State Chem.*, 1991, **28**, 131.
10 M. Roca, P. Amorós, J. Cano, M. Dolores Marcos, J. Alamo, A. Beltran-Porter and D. Beltran-Porter, *Inorg. Chem.*, 1998, **37**, 3167.
11 D. Massiot, H. Thiele and A. Germanus, *Bruker Winfit Report*, 1994, vol. 43, p. 140.
12 S. L. Wang, H. Y. Kang, C. Y. Cheng and K. H. Lii, *Inorg. Chem.*, 1991, **30**, 3496.
13 H. Y. Kang, W. C. Lee, S. L. Wang and K. H. Lii, *Inorg. Chem.*, 1992, **31**, 4743.
14 M. Roca, M. D. Marcos, P. Amorós, J. Alamo, A. Beltrán-Porter and D. Beltrán-Porter, *Inorg. Chem.*, 1997, **36**, 3414.
15 R. C. Haushalter, V. Soghomonian, Q. Chen and J. Zubieta, *J. Solid State Chem.*, 1993, **105**, 512.
16 K. H. Lii, L. S. Wu and H. M. Gau, *Inorg. Chem.*, 1995, **32**, 4153.
17 Y. Zhang, A. Clearfield and R. C. Haushalter, *J. Solid State Chem.*, 1995, **117**, 157.
18 P. Ayyappan, A. Ramanan and C. C. Torardi, *Inorg. Chem.*, 1998, **37**, 3628.
19 E. Le Fur and Y. Pivan J, *Mater. Res. Bull.*, 1999, **34**, 97.
20 E. Le Fur, O. Peña and J. Y. Pivan, *J. Alloys Compd.*, 1999, **285**, 89.
21 E. Le Fur and J. Y. Pivan, *J. Mater. Chem.*, 1999, **9**, 2589.
22 M. Schindler, W. Joswig and W. H. Baur, *J. Solid State Chem.*, 1999, **145**, 15.
23 I. D. Brown and D. Altermatt, *Acta Crystallogr., Sect. B*, 1985, **41**, 244.
24 S. Meyer, B. Mertens and H. k. Muller-Buschbaum, *Z. Naturforsch., Teil B*, 1997, **52**, 985.